

# The influence of radio-galaxy activity on X-ray absorption lines from the intracluster medium

Franziska Köckert<sup>1,2\*</sup> and Christopher S. Reynolds<sup>2</sup>

<sup>1</sup>*AIP, An der Sternwarte 16, D-14482 Potsdam, Germany.*

<sup>2</sup>*Dept. of Astronomy, University of Maryland, College Park, MD 20742, USA.*

arXiv:astro-ph/0602165v2 28 Mar 2006

Accepted 2006 January 31. Received 2006 January 24; in original form 2005 June 9

## ABSTRACT

We present an investigation of the X-ray absorption features predicted by hydrodynamic simulations of radio galaxies interacting with the intracluster medium (ICM) of their host galaxy clusters. We show how these absorption lines can be used as a new diagnostic for the radio-galaxy/ICM interactions. Such interactions have been observed in numerous systems by *ROSAT*, *Chandra* and *XMM-Newton*, and understanding them has implications for AGN feedback and galaxy formation. Starting from the hydrodynamic simulations of Reynolds, Heinz & Begelman, we calculate the properties of the highly ionized iron and oxygen lines (seen in absorption against the central active galactic nucleus; AGN), predicting line shapes, equivalent widths, column densities and velocity shifts. The main effect of the jet on the absorption lines is a reduction of the line strength from that of the quiescent ICM and the introduction of some velocity structure in the line profile. We investigate whether these features are detectable with current as well as future high-resolution X-ray spectrometers. We conclude that the *Chandra* transmission gratings have insufficient sensitivity to detect these features with high significance, and certainly would not allow a study of the dynamics of the interaction via absorption signatures. *Constellation-X*, on the other hand, will allow superb constraints to be derived. We can also use this analysis to assess the idea that radio-galaxy induced ICM outflows give rise to the resonant oxygen X-ray absorption lines that have been claimed as evidence for the warm-hot intergalactic medium (WHIM). We show that these detached, high-velocity oxygen absorption lines cannot result from a radio-galaxy/ICM interaction, thereby strengthening the WHIM interpretation.

**Key words:** galaxies: jets — intergalactic medium — line: profiles — shock waves — X-rays: galaxies: clusters

## 1 INTRODUCTION

It has been known for over a decade that radio galaxies at the cores of rich galaxy clusters interact with the surrounding intracluster medium (ICM) and, in some cases, influence it in significant and complex ways (e.g., Böhringer et al. 1993, 1995; Carilli, Perley & Harris 1994; Harris, Carilli & Perley 1994; Heinz, Reynolds & Begelman 1998). With the new generation of X-ray telescopes, *Chandra* and *XMM-Newton*, observations of these interactions have been more detailed than ever. For many systems it has been confirmed that there are cavities in the ICM which show up as depressions in the X-ray surface brightness and appear to be evacuated by the expanding radio lobes (e.g., Hydra-A; Mc-

Namara et al. 2000, Abell 2052; Blanton et al. 2001, Virgo-A; Young, Wilson & Mundell 2002, Perseus-A; Fabian et al. 2000, 2003a). Old radio lobes which have remained intact through magnetic or viscous effects (Reynolds et al. 2005, Kaiser et al. 2005, Jones & de Young 2005) are also believed to be responsible for the so-called “ghost” cavities seen in many clusters (e.g., Perseus, Fabian et al. 2003a; Abell 2597, McNamara et al. 2001; Abell 4059, Heinz et al. 2002, Choi et al. 2004). A second indication of the importance of radio-galaxy/ICM interactions is the cooling flow problem, that is the lack of cooled material in cluster cores despite the fact that the radiative cooling time of many ICM cores is rather short. Observations by *XMM-Newton* have shown that the gas does not in fact cool below 1–2 keV (the so-called temperature floor) begging us to identify a source of heating which can offset the radiative cooling.

\* E-mail: fkoeckert@aip.de (FK), chris@astro.umd.edu (CSR)

At the present time, the main observational diagnostics for radio-galaxy/ICM interactions are the spatial mapping in the X-ray band of temperature, pressure, cooling time and metal abundances of the ICM across the interaction region. However, with current data we lack any direct probe of the dynamics of the interaction, that is the velocities of the fluid disturbances, shocks and turbulence. A major hope for the *Suzaku* observatory was that it would open a direct window on the dynamics of these interactions through the velocity profiles of the ICM emission lines (Brüggen, Hoeft & Ruszkowski 2005); of course, the *Suzaku* cryostat failure and subsequent loss of the high-resolution X-ray Spectrometer (XRS) prevents this goal from being realized. Barring the emergence of a new mission possessing a high-resolution X-ray spectrometer, this important science goal must now await the launch of *Constellation-X*.

The current baseline design for *Constellation-X* has a requirement on the spatial resolution of 15 arcsec (half-power diameter). Coupled with its superior spectral resolution, this is sufficient to allow detailed mapping of radio-galaxy driven ICM dynamics through emission line profiles in the nearest systems such as the *Virgo* and *Perseus* clusters. For more distant systems, however, the interaction region is contained within a small number of spatial resolution elements, hampering the ability of the observation to constrain robust dynamical signatures. In this paper, we discuss the complementary technique of probing these radio-galaxy/ICM interactions through absorption line spectroscopy of the X-ray luminous core of the central radio galaxy, looking for jet-induced changes to the strength and line profile of the absorption lines present even in a static ICM. While detection and characterization of these absorption line features is more observationally demanding, it has the major advantage of probing the kinematic state of the gas through a well-defined ‘‘core sample’’ of the galaxy cluster, even if ones X-ray observatory has only limited spatial resolution. We focus on predictions of resonance K-shell absorption features of H- and He-like oxygen and iron arising in the ICM around an active as well as inactive radio galaxy, examining the velocity structure and strength of the lines.

These radio-galaxy/ICM interactions are particularly interesting and important since they appear to be the local and accessible examples of the more general phenomena of ‘‘AGN feedback’’ and potentially crucial for some aspects of cosmological structure formation (e.g., see Benson et al. 2003 and references therein). However, there is another important reason to study this phenomenon; it is of direct relevance to our observational understanding of the Warm-Hot Intergalactic Medium (WHIM). The filamentary WHIM is believed to be the repository for half of the baryons in the local Universe and so is of obvious interest to cosmologists. It is possible to detect the WHIM by wide field imaging of diffuse EUV and soft X-ray emission (see for example Kaasstra et al. 2003). However, the most important diagnostic of the WHIM are UV and X-ray absorption lines of oxygen seen in the spectra of bright AGN. Narrow oxygen OVI–OVI absorption lines at a redshift intermediate between zero and that of the AGN are taken to be good candidates for the WHIM. However, all AGN towards which such lines have been claimed are radio-loud AGN (see Section 5). The question arises whether these absorption line features are, in fact, outflows associated with the jetted AGN. While the

possibility remains that these features could be due to outflows associated with the central engine itself, we demonstrate that it is not possible to associate WHIM-like features with radio-galaxy/ICM interactions.

We predict the absorption line properties of radio-galaxy/ICM interactions by using the XSTAR photoionization code to post-process the hydrodynamics simulations of Reynolds, Heinz & Begelman (2002). Section 2 of this paper describes the underlying hydrodynamic simulations of the radio galaxy we use. Section 3 explains the simulation of our spectra using XSTAR. In Section 4, we summarize the properties (strengths and velocity structure) of the absorption lines that we predict as a function of the inclination with which we view the radio galaxy, the age of the radio-galaxy, and the properties of the ICM into which the radio-galaxy is expanding. Section 5 argues that these interactions cannot produce ‘‘WHIM-like’’ features, thereby strengthening the WHIM interpretation of these intermediate redshift absorption lines. Section 6 focuses on the ability of current future X-ray observatories to study these absorption lines and hence prove these radio-galaxy/ICM interactions. Finally, Section 7 presents our conclusions.

## 2 THE UNDERLYING HYDRODYNAMIC SIMULATIONS

The hydrodynamic simulation underlying this work is the canonical axisymmetric simulation of Reynolds, Heinz & Begelman (2002); for convenience, we briefly summarize the relevant details of the simulation here.

This 2-d hydrodynamic simulation explores the evolution of an active jet in a radio galaxy as it interacts with a surrounding ICM, and the resulting structure after the jet is shut down. Initially, we start with an isothermal spherical gaseous atmosphere with a (number) density profile given by

$$n(r) = \frac{n_0}{[1 + (r/r_0)^2]^{3/4}}. \quad (1)$$

The (fixed) gravitational potential is defined such that this atmosphere is in hydrostatic equilibrium. Back-to-back supersonic jets are injected in initial pressure balance with a density of  $n_{\text{jet}} = n_0/100$  and Mach number (with respect to the internal jet sound speed) of 10. The half-opening angle of the jet is  $15^\circ$ , and the starting point for the jets is a radius of  $r_0/20$ . As discussed in the Appendix of Reynolds, Heinz & Begelman (2002), this choice of parameters results in a cocoon in which the Kelvin-Helmholtz growth rates approximately match those calculated for real systems. Code units are related to physical units by parameters fixed to the background medium. For most runs we use the following canonical conversion factors:  $r_0 = 100 \text{ kpc}$ ,  $c_{\text{ISM}} = 1000 \text{ km s}^{-1}$ ,  $n_0 = 0.01 \text{ cm}^{-3}$  and  $T_0 = 4.4 \times 10^7 \text{ K}$ . This gives a total kinetic luminosity of the jets of  $9.3 \times 10^{45} \text{ erg s}^{-1}$ , making the simulation relevant for powerful radio sources located in rich galaxy clusters, like Cygnus A. We will refer to this as our ‘‘large cluster case’’. Since many radio galaxies are, however, found in smaller and cooler galaxy clusters, we also consider a different scaling ( $r_0 = 10 \text{ kpc}$ ,  $c_{\text{ISM}} = 500 \text{ km s}^{-1}$ ,  $n_0 = 0.05 \text{ cm}^{-3}$  and  $T_0 = 1.1 \times 10^7 \text{ K}$ ) which results in a total kinetic source luminosity of  $1.16 \times 10^{44} \text{ erg s}^{-1}$  and is

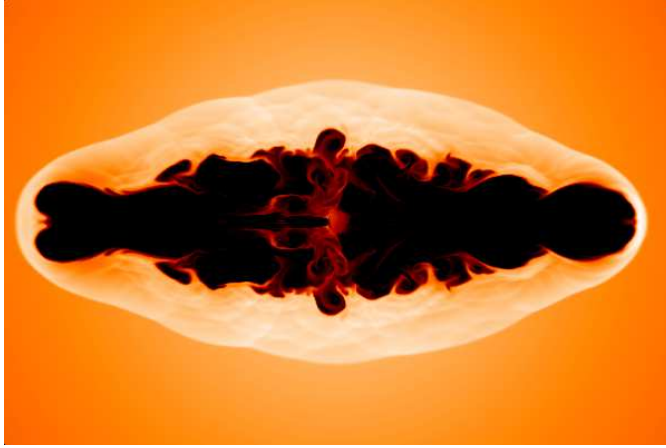


**Figure 1.** Density map of the jet and its close environment. In our large-cluster (“Cygnus-A”) scaling, the jet in this snapshot has been active for 30 Myr and the region displayed is the central  $200 \text{ kpc} \times 300 \text{ kpc}$  of the cluster.

closer to objects like Hydra A and Virgo A. We will refer to this as our “small cluster case”. In the first case, one code unit of time corresponds to 50 Myr. The total length of the simulation is 240 Myr, the jet is turned off after 50 Myr. In the second case, one code unit of time is 10 Myr, the total length is about 50 Myr, and the jet is turned off after 10 Myr. For more detailed information on the simulations, see Reynolds, Heinz & Begelman (2002). As an example of the simulation results, a density map is given in Fig. 1.

It is important to note that since these simulations were performed, Chandra observations have revealed several cases where the radio lobes of the central source are surrounded by a significant amount of cold gas. The ICM structures surrounding Perseus-A provide an excellent example (see Fabian et al. 2003a; Schmidt, Fabian & Sanders 2002). At the current time, the physical mechanisms underlying these cool rims are not understood and they cannot be reproduced in any first principles simulations. In systems containing such rims, the observed oxygen OVII and OVIII absorption lines towards the central AGN are likely to be dominated by the contribution from gas in the rim; according to Schmidt, Fabian & Sanders (2002), the temperature and density in the cold gas rim of the Perseus cluster are  $3.6 \times 10^7 \text{ K}$  and  $0.12 \text{ cm}^{-3}$  respectively. Using simple calculations based on Shull & van Steenberg (1982), this gives an OVIII equivalent width of 0.15 eV, larger than that predicted from the entire rest of the ICM atmosphere. Therefore, our results presented here are valid only for systems that do not possess these cold rims, or for lines of sight that do not intercept such rims.

### 3 SIMULATION OF THE ABSORPTION FEATURES

The hydrodynamic simulation gives us the density, temperature and velocity of the ICM at every point in space as a function of time throughout the modelled radio-galaxy/ICM interaction. To simulate the absorption line spectrum that one would see towards the central radio galaxy, we used the photoionization code XSTAR (developed by Tim Kallman; see Kallman & Bautista 2001) to calculate the opacity of

the ICM along radial rays that originate at the AGN. We assume a collisionally-ionized plasma in thermal and ionization equilibrium. These assumptions are readily verified for the ions of interest.

We take the temperature, density and velocity directly from the hydrodynamic simulation. The frequency-dependent opacity is calculated including both thermal line broadening and line-of-sight Doppler shifts. We choose an energy resolution of  $\Delta E/E = 3.29 \times 10^{-4}$ , giving a velocity resolution of about 100 km/s.

XSTAR includes 13 elements, and the elemental abundances are important for the resulting line spectrum. We chose abundances measured by Allen & Fabian (1998), Loewenstein & Mushotzky (1996) and Baumgartner et al. (2005), which we summarize in Table 1.

All publicly available photoionization codes have some problems dealing with very low densities and very high temperatures ( $> 10^9 \text{ K}$ ); XSTAR is no exception. However, such high temperatures only occur in early times of the simulations, when the jet is still on, and then only in the innermost grid cells, very close to the source. We can safely ignore those cells (through the inclusion of a threshold temperature above which the simulation cell is skipped) since very high temperature gas has no line absorption anyway. The only case where a considerable number of grid cells is affected is along the jet-axis  $\theta < 1^\circ$ . Due to the forced symmetry of the simulations the region  $\theta < 1^\circ$  is unphysical because material gets “stacked” on the jet axis. The minimum line-of-sight angle that we choose to analyze is  $\theta = 5.5^\circ$ , appropriate for blazar-type sources.

### 4 RESULTS

In this section, we discuss the impact that the radio-galaxy activity has on the observed X-ray absorption lines in our simulated system. The astrophysical relevance of these results, and the ability of current and future instruments to measure the predicted absorption lines will be addressed in the following sections.

We performed two sets of absorption line simulations. The first set examines different lines of sight towards the AGN, at four chosen times of the jet evolution. Using the large cluster case, we chose to examine the spectrum of the system at 30 Myr (when the jet is fully active), at 50 Myr (just when the jet is turned off), 100 Myr (well after it is turned off) and at the end of the simulation at 240 Myr. Our second set of calculations looks at the continuous evolution in time, along five representative lines of sight which make an angle  $\theta = 5.5, 12, 30, 60$  and  $90$  degrees with the jet axis.

While our calculations actually include the thousands of lines that are incorporated into XSTAR, we focus our examination on the K-shell resonant absorption lines of FeXXV (6.70 keV), OVII (0.574 keV) and OVIII (0.654 keV) lines since these are expected to be the strongest and/or most interesting. After examining the possibility of observing the features with *Constellation-X*, we decided to also carefully examine the SiXIII line (1.86 keV) since it turned out to be particularly strong and at an energy that is particularly well-tuned to *Constellation-X*. We note that the FeXXVI lines (6.95 keV and 6.97 keV) will not be discussed in much detail since they prove too weak to be detected even with

Element	C	N	O	Ne	Mg	Si	S	Ar	Ca	Fe	Ni
$Z/Z_{\odot}$	0.34 <sup>a</sup>	0.34 <sup>a</sup>	0.48 <sup>b</sup>	0.62 <sup>b</sup>	0.376 <sup>b</sup>	0.63 <sup>c</sup>	0.26 <sup>c</sup>	0.17 <sup>c</sup>	0.275 <sup>c</sup>	0.401 <sup>c</sup>	1.02 <sup>c</sup>

**Table 1.** Cosmic element abundances compared to solar. <sup>a</sup>Allen & Fabian 1998, <sup>b</sup>Loewenstein & Mushotzky 1996, <sup>c</sup>Baumgartner et al. 2005

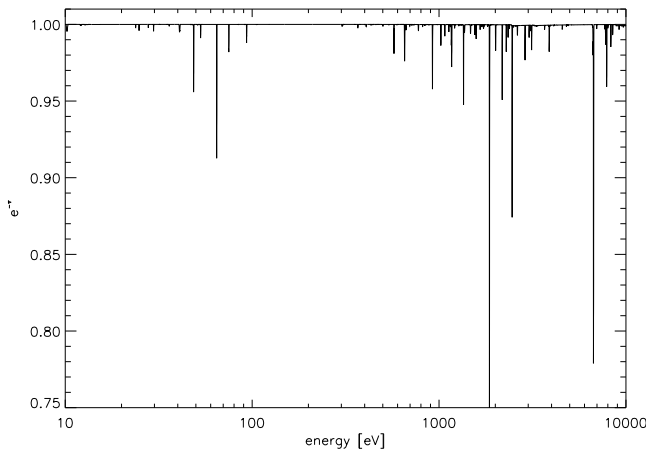


**Figure 2.** The simulated XSTAR spectrum for  $\theta = 5.5^\circ$  and  $t=50$  Myr (large-cluster case).

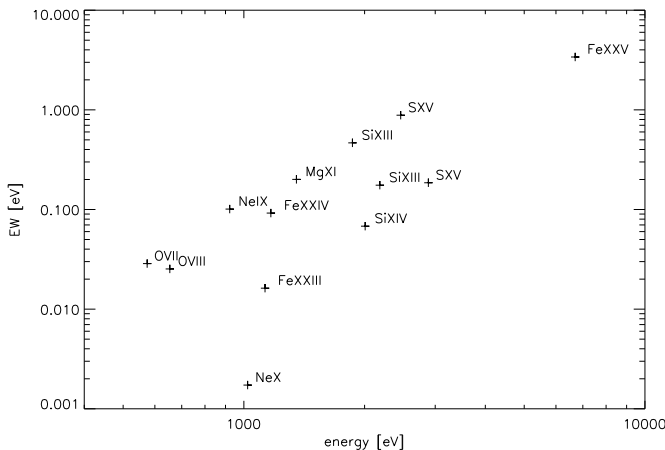


**Figure 3.** The strength of the most prominent lines in the simulated spectrum for  $\theta = 5.5^\circ$  and  $t = 50$  Myr (large-cluster case).

*Constellation-X.* For all cases, we examine the optical depth, equivalent width, column density and velocity shifts. Figure 2 shows an example for the simulated full spectrum for  $\theta = 5.5^\circ$ ,  $t=50$  Myr (large cluster case). Figure 3 shows the strengths of the most prominent lines in this case.

#### 4.1 The undisturbed material

Even the undisturbed ICM produces significant oxygen and iron line absorption (Krolik & Raymond 1988; Sarazin 1989). Undisturbed lines arise from material which is either ahead of the shock front, or which has settled down again since enough time has passed since the jet was turned off. For

our large cluster case, the FeXXV and FeXXVI equivalent widths are 11.65 eV and 0.086 eV (corresponding to column densities of  $N_{\text{FeXXV}} = 1.32 \times 10^{17} \text{ cm}^{-2}$  and  $N_{\text{FeXXVI}} = 2.81 \times 10^{15} \text{ cm}^{-2}$ ) whereas for OVII, OVIII and SiXIII we predict 0.05 eV, 0.155 eV and 1.536 eV (corresponding to column densities of  $N_{\text{OVII}} = 6.46 \times 10^{14} \text{ cm}^{-2}$ ,  $N_{\text{OVIII}} = 1.68 \times 10^{15} \text{ cm}^{-2}$  and  $N_{\text{SiXIII}} = 1.84 \times 10^{16} \text{ cm}^{-2}$ ).

For the small cluster case, there is no FeXXVI line since the ICM does not get hot enough for appreciable H-like iron to exist. FeXXV and SiXIII have equivalent widths of 7.64 eV and 11.97 eV (corresponding to column densities of  $N_{\text{FeXXV}} = 8.67 \times 10^{16} \text{ cm}^{-2}$  and  $N_{\text{SiXIII}} = 1.43 \times 10^{17} \text{ cm}^{-2}$ ), OVIII and OVII have equivalent widths of 1.004 eV and 0.548 eV (corresponding to column densities of  $N_{\text{OVIII}} = 1.1 \times 10^{16} \text{ cm}^{-2}$  and  $N_{\text{OVII}} = 7.12 \times 10^{15} \text{ cm}^{-2}$ ). The oxygen and SiXIII lines are stronger than in the large-cluster case since there is more cooler material to contribute to the absorption, but the FeXXV line is weaker due to the low assumed temperature of the ICM.

#### 4.2 Disturbances introduced by the jet

When the AGN jet moves through the ICM, it influences it in numerous ways. First, it can induce motions in large amounts of material. As the ICM gets swept up in the shock-front, some of it moves outwards with the shocked shell and some gets caught in a backflow. In the late stages of the evolution of the system, a significant amount of ICM falls back into the core regions as the cocoon collapses and buoyantly rises into the cluster atmosphere. All of these effects will imprint signatures (broadening, and the development of blueshifted and redshifted wings and peaks) in the absorption line profiles. The second strong effect is a change of the ICM temperature. Strong shocks associated with the early phase of jet activity will appreciably heat some regions of the ICM, typically raising it to temperatures sufficient to fully ionize oxygen. On the other hand, unshocked ICM that is caught in the ‘‘updraft’’ from a buoyant cocoon will adiabatically decompress and be cooled (strengthening oxygen absorption features).

Clearly, the kinematics and the thermodynamics are coupled. We might expect (and, as discussed below, confirm) it to be appreciably harder to form high velocity oxygen absorbers than iron absorbers, since any strong shock responsible for accelerating the gas will inevitably heat it to the point where oxygen becomes fully ionized. On the other hand, we find iron lines which, in the strongest cases, display a double peak structure, with one peak being at the rest energy of the line and one being clearly blueshifted but still attached to the line itself. In those cases, the blueshifted components arise from a large amount of shock accelerated material outflowing at fairly high speeds, whereas the peak at the rest energy comes from still undisturbed material in front of the jet.

Representative results for oxygen and iron line profiles and equivalent widths are shown in Figs. 4–7. It is instructive to separate the discussion of the *cocoon inflation* phase of activity from that of the *cocoon collapse and buoyant plume formation* phase. During the cocoon inflation phase, the radio galaxy activity inflates an over-pressured cocoon which, in turn, drives a strong shock into the ICM. The high ICM temperatures produced by this shock leads to a rapid drop in the equivalent widths of the OVII, OVIII, SiXIII and FeXXV lines with rather little change in the line profile. The decrease in line equivalent widths are rather more dramatic for lines of sight close to the jet axis simply due to the increased path-length along which the ambient line-absorbing ICM has been scoured out by the cocoon shock.

Towards the end of the cocoon-inflation phase, the cocoon pressure becomes comparable to that of the ambient ICM and the shock weakens. After that, the source transits into the cocoon-collapse phase in which the shocked ICM surrounding the sides of the cocoon (i.e., the equatorial regions with respect to the jet axis) falls back towards the cluster center. The result of this infall is to “squeeze” the cocoon plasma and transform it into two buoyantly rising, mushroom-shaped plumes (see Fig. 1 of Reynolds, Heinz & Begelman 2002). During these times, the equivalent widths of the OVII, OVIII, SiXIII and FeXXV absorption lines gradually recover to approximately their initial values. However, the complex dynamics of the ICM during this phase create imprints in the line profiles. For lines of sight close to the jet axis, both the oxygen and iron absorption lines develop blue wings corresponding to absorption by the outward moving ICM shell and, latter, ICM that is being dragged out of the core regions of the cluster in the wake of the buoyant ICM plume. These features are subtle in the case of the oxygen lines, but are rather dramatic in the case of the FeXXV lines. In all cases, the velocities characterizing the blue-wing are less than but of the order of the ICM sound speed. Interestingly, for lines of sight that make a large angle with the jet-axis, the FeXXV line displays a subtle redshift of its centroid corresponding to the actual inward collapse of the ICM core (Fig. 7).

## 5 IMPLICATIONS FOR THE WHIM OBSERVATIONS

There has been much recent excitement about the possible detection of the WHIM through the OVII and OVIII K-shell resonant absorption lines. This is of obvious importance given that these WHIM filaments are expected to be the repository for half of the baryons in the local Universe. The most robust detection to date was obtained by a *Chandra* High Energy Transmission Gratings (HETG) observation of the blazar Mrk 421 during an outburst (Nicastro et al. 2005a,b). Two absorber systems were detected in both OVII and NVII at velocities of  $cz = 3300 \pm 300 \text{ km s}^{-1}$  and  $cz = 8090 \pm 300$  (to be compared with the recession velocity of the blazar of  $CZ = 9000 \text{ km s}^{-1}$ ). The OVII  $K\alpha$  EWs of these two systems were measured to be  $0.080 \pm 0.021 \text{ eV}$  ( $3.0 \pm 0.8 \text{ m}\text{\AA}$ ) and  $0.059 \pm 0.021 \text{ eV}$  ( $2.2 \pm 0.8 \text{ m}\text{\AA}$ ). Nicastro et al. (2005b) demonstrate that the column density distribution implied by these detections is consistent with the notion that the WHIM filaments do, indeed, balance the

baryon budget of the local Universe. While this is the most robust detection of  $z > 0$  WHIM, it was not the first. Fang et al. (2002) claim a detection of the OVIII  $K\alpha$  line with an EW of  $0.41 \text{ eV}$  from a system with  $cz = 16,600 \text{ km s}^{-1}$  towards the blazar PKS 2155–304 (which has a systemic velocity of  $cz = 34,800 \text{ km s}^{-1}$ ), although the significance of this detection (which is based on finding a single line in a blind search of the spectrum) has been questioned. McKernan et al. (2003) also claim a OVIII line with a velocity of  $cz = 4400 \text{ km s}^{-1}$  and a EW of  $2.17 \text{ eV}$  towards the broad line radio galaxy 3C120 (which has a systemic velocity of  $cz = 9900 \text{ km s}^{-1}$ ). Other recent detections of  $z > 0$  WHIM via X-ray absorption lines have been reported towards the BL-Lac object PKS 0548–322 (Barcons et al. 2005) and the radio-loud quasar H1821+643 (Mathur, Weinberg & Chen 2003).

While observational biases are evident, it is striking that all of the claimed detections of  $z > 0$  WHIM are along lines of sight towards radio-loud AGN. The question arises as to whether some aspect of jetted AGN can produce high-velocity and detached X-ray absorption lines. With our calculations, we can address one particular class of models, i.e., those where the high-velocity X-ray absorption lines are produced in an jet-induced ICM outflow. In particular, we search for phases of activity in which one would see narrow and detached oxygen absorption lines. In fact, at no point in time do we ever see such features. Instead, any high velocity material always appears as a blueshifted tail on the main zero velocity absorption line. Furthermore, our velocity shifts are on the order of the sound speed in our ICM. Any ICM that is accelerated to appreciably higher velocities will be shock heated to a point where it can no longer produce oxygen absorption lines (i.e., the oxygen will be fully ionized).

Thus, we conclude that the observed WHIM-like absorption line systems cannot arise from ICM/jet interactions. This leaves two possibilities. One would be nuclear absorption, meaning absorption from outflowing material in the central nucleus of the AGN, for example from an accretion disk wind. This could be tested by looking for variability of the line, since the region of origin would be comparatively small. The other possible explanation remains the WHIM. It is important to obtain deep high-resolution spectra of radio-quiet AGN in order to assess this possibility.

## 6 OBSERVING ABSORPTION LINES RESULTING FROM ICM-RG INTERACTIONS

We have used the XSPEC spectral fitting package to investigate the possibility of observing our simulated absorption features with *Chandra*, *Suzaku* and *Constellation-X*. To simulate ICM absorption towards a bright radio-galaxy, we use our calculations to predict the absorption towards a power-law source with photon index  $\Gamma = 1.6$  and flux  $3 \times 10^{-11} \text{ erg cm}^{-2} \text{ s}^{-1}$ . These parameters are chosen to mimic the radio-galaxy 3C 120 (McKernan et al. 2003). Note that while our hydrodynamic simulations were motivated by Cygnus-A, the highly absorbed nature of the nucleus of Cygnus-A makes it inappropriate as a target for such absorption line studies. Given a predicted spectrum, we use

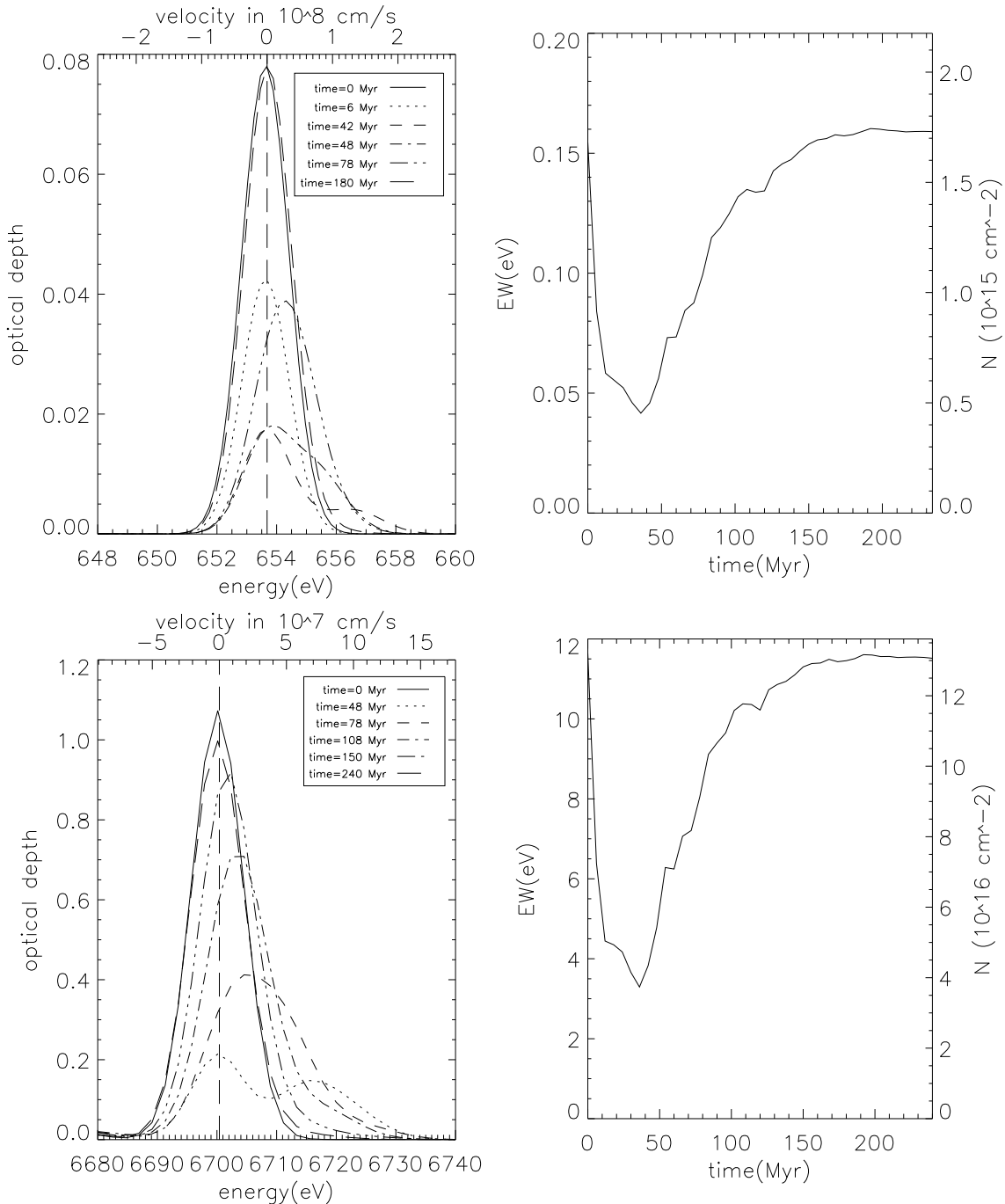


**Figure 4.** Line profiles and equivalent widths as a function of time for the small inclination case of  $\theta = 5.5^\circ$  and the large-cluster scaling. *Upper left panel*: Energy profiles of the OVIII K $\alpha$  resonance absorption line. *Upper right panel* : Total equivalent width of the OVIII K $\alpha$  resonance absorption line as a function of time. *Lower left panel*: Energy profile of the FeXXV K $\alpha$  resonance absorption line. *Lower right panel*: Total equivalent width of the FeXXV absorption lines as a function of time. Note the growth of an extended blue-shifted wing at the end of the cocoon-inflation phase.

the “fakeit” tool in XSPEC to simulate spectra using the appropriate response matrices for the high-energy transmission gratings (HETG) on *Chandra*, the now in-operable X-ray spectrometer (XRS) on *Suzaku* and the microcalorimeter on *Constellation-X*. We chose the optimistic case of integration times of 200 ks.

To determine the detectability of the lines of interest,

we first fitted the simulated data with a powerlaw. We then search for the absorption lines by adding a simple negative Gaussian model and applying the F-test to the resulting improvement in the goodness of fit. This procedure reveals that neither *Chandra*/HETG nor *Suzaku*/XRS are able to detect the iron and oxygen absorption features for lines-of-sight close to the jet axis, because along those lines-of-sight the

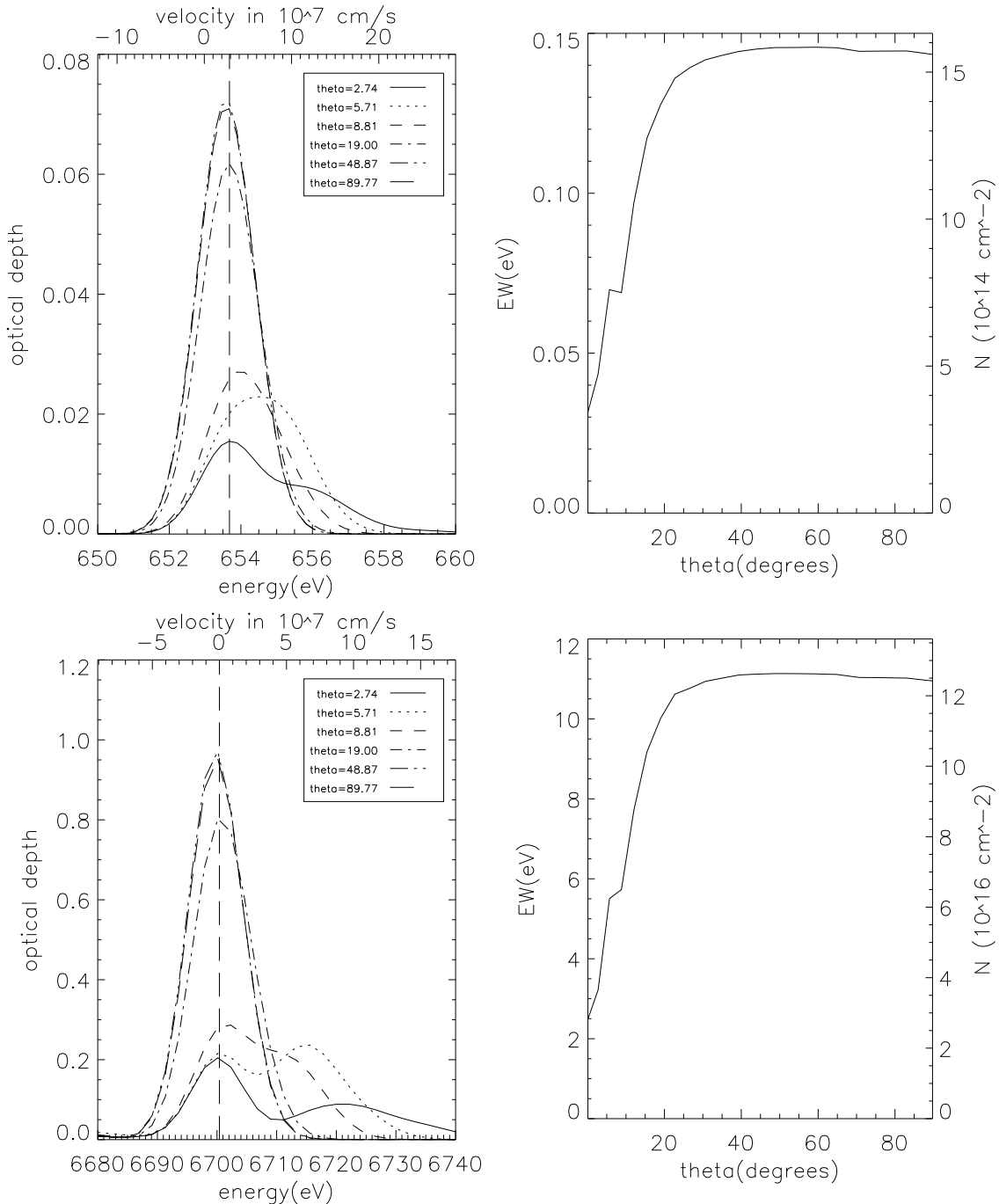


**Figure 5.** Line profiles and equivalent widths as a function of viewing angle at the time that the jet shuts off ( $t = 50$  Myr) for the large-cluster scaling. *Upper left panel*: Energy profiles of the OVIII K $\alpha$  resonance absorption line. *Upper right panel* : Total equivalent width of the OVIII K $\alpha$  resonance absorption line as a function of inclination. *Lower left panel*: Energy profile of the FeXXV K $\alpha$  resonance absorption line. *Lower right panel*: Total equivalent width of the FeXXV absorption lines as a function of inclination. Note the growth of an extended blue-shifted wing at small inclinations.

predicted features are also the weakest. The only detectable feature at  $\theta = 5.5^\circ$  is the SiXIII line. The simulated line as detected by *Suzaku* is shown in Fig. 8. Detections of the other features with *Suzaku* are possible at higher inclinations. As discussed in Section 4 however, the ICM dynamics imprint only subtle features on the line profile for these higher inclinations. Thus, we conclude that studies of ICM

dynamics using these absorption lines are not possible with the current generation of instruments.

On the other hand, NASA's proposed *Constellation-X* observatory will have such improved sensitivity that it will easily allow the study of jet-driven ICM dynamics using absorption line profiles. Looking at the case of  $\theta = 5.5^\circ$  and  $t=50$  Myr, the most prominent lines picked

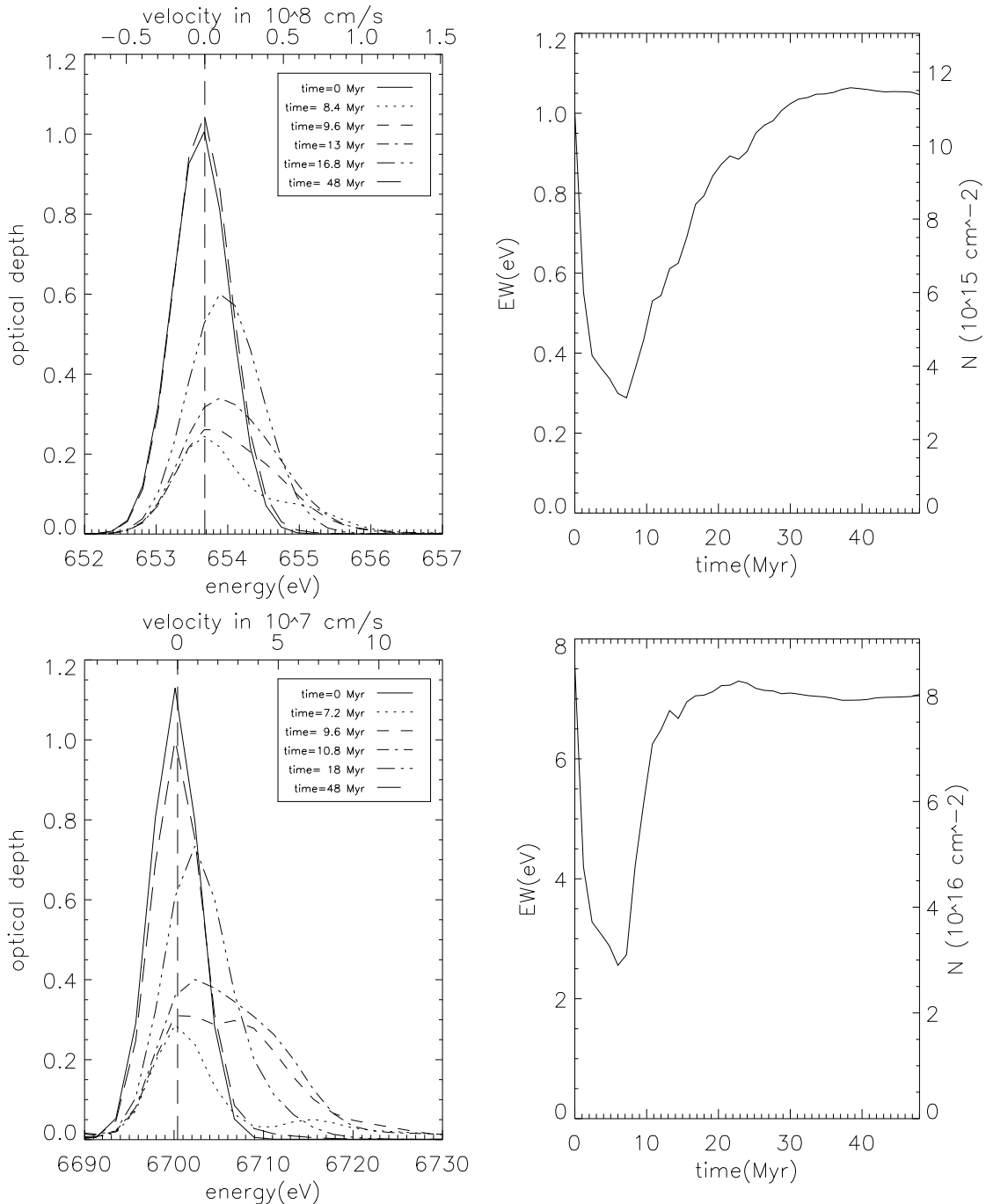


**Figure 6.** Line profiles and equivalent widths as a function of time for the small inclination case of  $\theta = 5.5^\circ$  and the small-cluster scaling. *Upper left panel:* Energy profiles of the OVIII K $\alpha$  resonance absorption line. *Upper right panel :* Total equivalent width of the OVIII K $\alpha$  resonance absorption line as a function of time. *Lower left panel:* Energy profile of the FeXXV K $\alpha$  resonance absorption line. *Lower right panel:* Total equivalent width of the FeXXV absorption lines as a function of time. Note the growth of an extended blue-shifted wing at the end of the cocoon-inflation phase.

up by *Constellation-X* are SiXIII, FeXXV, SXV, MgXI, FeXXIV, NeIX, OVIII, NeX and OVII. As shown in Fig. 9, FeXXV displays the double peaked structure with one strongly blueshifted second peak introduced by the outflowing shocked ICM shell. SiXIII and SXV both display blueshift wings making a Gaussian not an adequate model anymore. All lines display blueshifted peaks with  $\Delta v = 10^6$

to  $10^7 \text{ cm s}^{-1}$ . The simulated FeXXV line detection is shown in Fig. 9.

## 7 CONCLUSIONS

In this paper we present spectral simulations of ICM absorption features arising from radio-galaxy/ICM interactions.

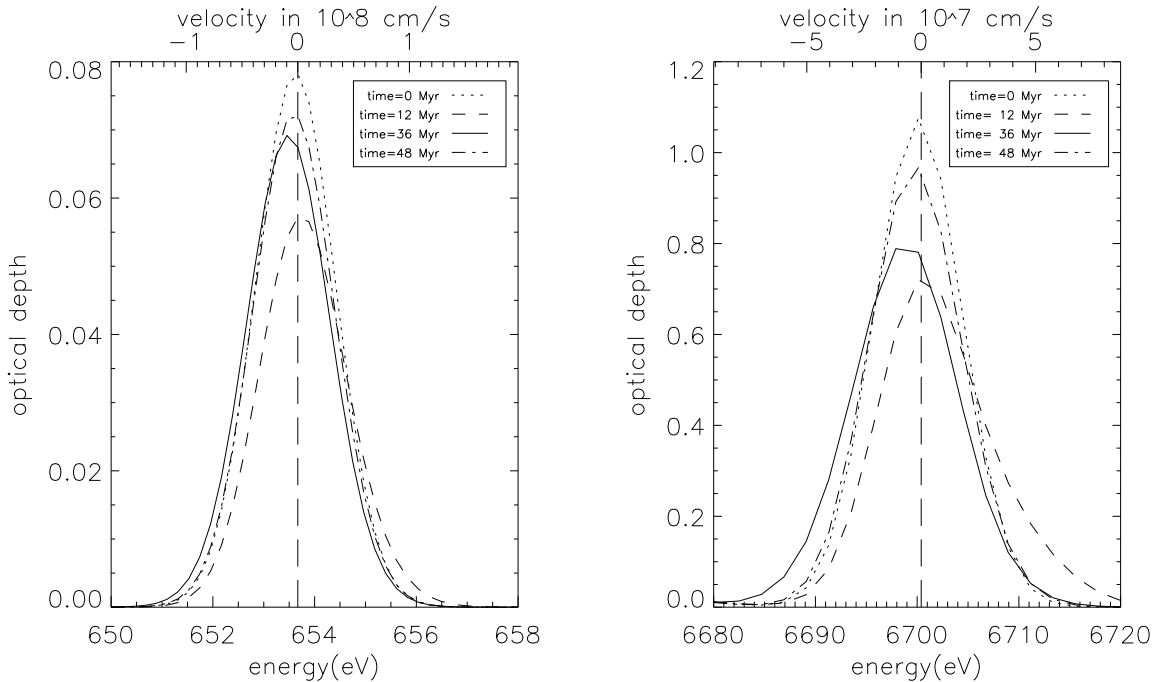


**Figure 7.** Line profiles and equivalent widths as a function of time at a viewing angle of  $60^\circ$  for the large-cluster scaling. *Left panel:* Energy profiles of the OVIII K $\alpha$  resonance absorption line. *Right panel:* Energy profile of the FeXXV K $\alpha$  resonance absorption line. Note the subtle redshift of the centroid of both lines associated with the lateral collapse of the cocoon, at  $t=36$  Myr (solid line).

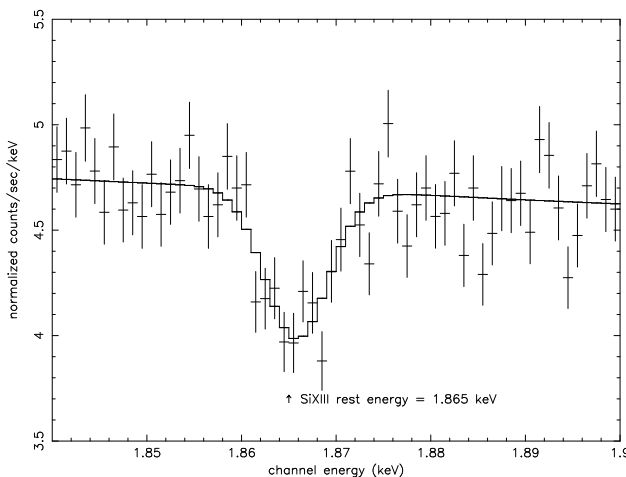


**Figure 8.** Simulated *Suzaku* detection of the SiXIII line in the large-cluster case for an inclination of  $\theta = 5.5^\circ$ , and a time of  $t = 50$  Myr. See text for details of the simulated source and observation.

These features can be used as a new tool to probe interactions between the ICM and radio galaxies. The energy introduced by the jet weakens the lines already present due to the static ISM and, more importantly, introduces a velocity structure in the form of wings and blueshifted line peaks in the line profile. We specifically looked at OVIII, OVII and FeXXV. The results were quantified as equivalent widths, column densities and velocity shifts of those absorption lines. We used the results for the oxygen lines to test the possibility of jet-induced ICM outflow giving rise to absorption lines which could be mistaken as WHIM in the claimed ob-

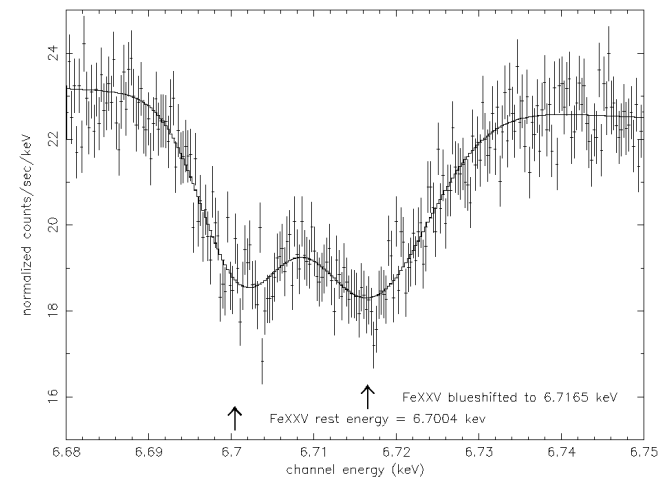


**Figure 9.** Simulated *Constellation-X* detection of FeXXV in the large-cluster case for an inclination of  $\theta = 5.5^\circ$ , a time of  $t = 50$  Myr. See text for other details of the simulated source. Note the double-peak structure. The blueshifted peak corresponds to material in the approaching shocked-shell of ICM.

servations. Our results largely rule that out and strengthen the WHIM interpretation. We also tested the possibility of actually observing those features introduced by the jet with the HETG on *Chandra*, the now inoperable XRS on *Suzaku* and the microcalorimeter on *Constellation-X*. *Chandra* is not sensitive enough to detect the features. *Suzaku* would have been barely sensitive enough to detect SiXIII and FeXXV, but only along lines of sight fairly far away from the jet axis, where the jet influence is minimal and therefore it is not possible to learn much about the interaction dynamics between

the AGN and the ICM. *Constellation-X* will have a vastly superior sensitivity and is therefore much more suitable for that task. In our simulations, *Constellation-X* readily detects these features, can detect double-peaked FeXXV lines resulting from the expanding shocked ICM shell, and can detect the re-collapse of the inner ICM after the AGN has turned off. We suggest that such observations may be a powerful new diagnostic of the dynamics of radio-galaxy/ICM interactions.

## 8 ACKNOWLEDGMENTS

We thank Tim Kallman, Barry McKernan and John Verneraleo for stimulating conversations throughout the course of this work. We also thank the referee, Professor Claude Canizares, for a thorough and thoughtful critique of the original manuscript. CSR gratefully acknowledges support from the National Science Foundation under grant AST0205990 and from the *Chandra* Cycle-5 Theory & Modelling program under grant TM4-5007X.

## REFERENCES

Allen, S.W., Fabian, A.C., 1998, MNRAS, 297, 63  
 Barcons X., Paerels F.B.S., Carrera F.J., Ceballos M.T., Sako M., 2005, MNRAS, 359, 1549  
 Baumgartner, W.H., Loewenstein, M., Horner, D.J., Mushotzky, R.F., 2005, ApJ, 620, 680  
 Benson A.J., Bower R.G., Frenk C.S., Lacey C.G., Baugh C.M., Cole S., 2003, ApJ, 599, 38  
 Blanton E.L., Sarazin C.L., McNamara B.R., Wise M.W., 2001, ApJ, 558, L15  
 Böhringer H., Voges W., Fabian A.C., Edge A.C., Neumann D.M., 1993, MNRAS, 264, L25  
 Böhringer H., Nulsen P.E.J., Braun R., Fabian A.C., 1995, MNRAS, 274, L67  
 Brüggen M., Hoeft M., Ruszkowski M., 2005, ApJ, 628, 153  
 Carilli C.L., Perley R.A., Harris D.E., 1994, MNRAS, 270, 173  
 Choi Y.Y., Reynolds C.S., Heinz S., Rosenberg J.L., Perlman E.S., Yang J., 2004, ApJ, 606, 185  
 Fabian A.C. et al., 2000, MNRAS, 318, L65  
 Fabian A.C., Sanders J.S., Allen S.W., Crawford C.S., Iwasawa K., Johnstone R.M., Schmidt R.W., Taylor G.B., 2003, MNRAS, 344, L43  
 Fang, T., Marshall, H.L., Lee, J.C., Davis, D.S., Canizares, C.R., 2002, ApJ, 572, L127  
 Harris D.E., Carilli C.L., Perley R.A., 1994, Nat, 367, 713  
 Heinz S., Reynolds C.S., Begelman M.C., 1998, ApJ, 501, 126  
 Heinz S., Choi Y.Y., Reynolds C.S., Begelman M.C., 2002, ApJ, 569, L79  
 Jones T., de Young D.S., 2005, ApJ, 624, 586  
 Kaastra J.S., Lieu R., Tamura T., Paerels F.B.S., den Herden J.W., 2003, A&A, 397, 445  
 Kallman, T.R., Bautista, M.A., 2001, ApJS, 133, 221K  
 Kaiser, C.R., Pavlovski, G., Pope, E.C.D., Fangohr, H., 2005, MNRAS, 359, 493  
 Krolik J.H., Raymond J.C., 1988, ApJL, 335, L39  
 Loewenstein, M., Mushotzky, R.F., 1996, ApJ, 517, 108  
 Mathur S., Weinberg D.H., Chen X., 2003, ApJ, 582, 82  
 McKernan, B., Yaqoob, T., Mushotzky, R., George, I.M., Turner, T.J., 2003, ApJ, 598, L83  
 McNamara B.R. et al., 2000, ApJ, 534, L135  
 McNamara B.R. et al., 2001, ApJ, 562, L149  
 Nicastro F., et al., 2005a, ApJ, 629, 700  
 Nicastro F., et al., 2005b, Nat, 433, 495  
 Reynolds, C.S., Heinz, S., Begelman, M.C., 2002, MNRAS, 332, 271  
 Reynolds, C.S., McKernan, B., Fabian, A.C., Stone, J.M., Verneraleo, J.C., 2005, MNRAS, 357, 242  
 Sarazin C.L., 1989, ApJ, 345, 12  
 Schmidt R.W., Fabian A.C., Sanders J.S., 2002, MNRAS, 337, 71  
 Shull J.M., van Steenberg M., 1982, ApJS, 48, 95  
 Young A.J., Wilson A.S., Mundell C.G., 2002, ApJ, 579, 560